

Evolution of the resistivity anisotropy in $\text{Bi}_2\text{Sr}_{2-x}\text{La}_x\text{CuO}_{6+\delta}$ single crystals for a wide range of hole doping

S. Ono and Yoichi Ando*

Central Research Institute of Electric Power Industry, Komae, Tokyo 201-8511, Japan

(Dated: February 7, 2020)

To elucidate how the temperature dependence of the resistivity anisotropy of the cuprate superconductors changes with hole doping, both the in-plane and the out-of-plane resistivities (ρ_{ab} and ρ_c) are measured in a series of high-quality $\text{Bi}_2\text{Sr}_{2-x}\text{La}_x\text{CuO}_{6+\delta}$ (BSLCO) single crystals over a wide range of x ($0.23 \leq x \leq 1.02$), which corresponds to the hole doping per Cu, p , of 0.03 – 0.18. It is found that the ρ_c/ρ_{ab} ratio shows a systematic increase with decreasing p at moderate temperatures, except for the most underdoped composition where the localization effect enhances ρ_{ab} and thus lowers ρ_c/ρ_{ab} . At room temperature, the change in ρ_c/ρ_{ab} is weak for $p = 0.14 – 0.18$, but it increases quickly for $p \leq 0.12$ with decreasing p ; we discuss that this behavior comes from the effect of the pseudogap which causes ρ_c/ρ_{ab} to be increasingly more enhanced as p is reduced in underdoped samples. The pseudogap also causes a rapid growth of ρ_c/ρ_{ab} with decreasing temperature, and, as a result, the ρ_c/ρ_{ab} value almost reaches 10^6 in underdoped samples just above T_c . The whole data set from BSLCO demonstrates that the resistivity anisotropy of the cuprates is determined by three mechanisms, namely, charge confinement, pseudogap, and localization.

PACS numbers: 74.25.Fy, 74.25.Dw, 74.72.Hs

I. INTRODUCTION

It has long been recognized that the peculiar c -axis transport properties¹ of the high- T_c cuprates are strong manifestations of the unusual electronic state in these materials.² In particular, the following two features have been considered to be most unusual: (i) The magnitude of the c -axis resistivity ρ_c is orders of magnitude larger than that expected from band calculations,³ leading to a huge resistivity anisotropy where ρ_c is up to 10^5 times larger⁴ than the in-plane resistivity ρ_{ab} . (ii) The temperature dependence of ρ_c is in most cases semiconducting or insulating (i.e., $d\rho_c/dT < 0$), while that of ρ_{ab} is metallic ($d\rho_{ab}/dT > 0$); such a contrasting behavior^{5,6,7} is not expected in ordinary anisotropic metal.^{1,2}

The feature (i) indicates that the strong correlations in the cuprate materials give rise to some unconventional mechanism which renormalizes the c -axis transfer-matrix element to a value much smaller than what is expected for an uncorrelated system. This renormalization of the c -axis transfer-matrix element is usually called “charge confinement”. There have been many theoretical proposals to explain the charge confinement in the cuprates, but it is fair to say that the confinement mechanism is not yet understood on the fundamental level. Since many of the theoretical models for the charge confinement, such as the resonating-valence-bond theories^{8,9} or self-organized stripe theories,^{10,11} are closely tied to the mechanism of the high- T_c superconductivity, it remains to be important to study the c -axis transport in the cuprates.

The feature (ii) is now better understood than the feature (i), both experimentally and theoretically, though the understanding is still far from complete. To appreciate the current understanding of the feature (ii), it should first be recognized¹² that the c -axis transport in the normal-state of the cuprates is essentially an incoher-

ent tunneling process; this fact gives rise to the intrinsic Josephson effect¹³ as well as the Josephson-plasma resonance¹⁴ in the superconducting state. It should at the same time be noted that the tunneling conductance for ordinary metal-insulator-metal junctions should be *independent* of temperature, according to the Fermi golden rule; this means that the “semiconducting” behavior of $\rho_c(T)$ does *not* automatically arise from the tunneling nature of the c -axis transport. (In this sense, the expression “semiconducting behavior”, which implies that the transport is essentially an activation process over a gap, is inappropriate, though this expression is often naively used in this context.) Thus, there must be some unconventional mechanisms which cause the peculiar “insulating” temperature dependence of ρ_c in the cuprates.

Experimentally, there seem to be two additive mechanisms that are both responsible for the “insulating” $\rho_c(T)$. The first is the charge-confinement mechanism which appears to become increasingly more effective with lowering temperature; this causes the tunneling matrix element to be reduced and keeps ρ_c to be increasing. This point was most clearly demonstrated⁷ by the low-temperature normal-state resistivity measurement of $\text{Bi}_2\text{Sr}_{2-x}\text{La}_x\text{CuO}_{6+\delta}$ (BSLCO) under 60 T, which showed that ρ_c of Bi-2201 keeps increasing even down to 0.6 K. The more recently recognized mechanism is the effect of the pseudogap¹⁵ which causes destruction of the Fermi surface starting from the $(\pm\pi, 0)$, $(0, \pm\pi)$ points, as has been demonstrated by angle-resolved photoemission spectroscopy (ARPES) measurements¹⁶; this causes the available density of states for tunneling to be reduced, and ρ_c gets steeply increased as the pseudogap develops. Note that the c -axis matrix element of the cuprates has a particular \mathbf{k} -dependence¹⁷ (\mathbf{k} is the in-plane wave vector of the conduction electrons) that tends to amplify the contribution of the elec-

trons on these gapped portion of the Fermi surface, and this \mathbf{k} -dependence of the matrix element causes ρ_c to be very sensitive to the opening of the pseudogap.¹² Recent tunneling-spectroscopic studies^{18,19} of the intrinsic junctions in $\text{Bi}_2\text{Sr}_2\text{CaCu}_2\text{O}_{8+\delta}$ (Bi-2212) have made strong cases for the interpretation that the steep upturn in $\rho_c(T)$ below the pseudogap temperature T^* is largely due to this second mechanism. It is expected that these two independent mechanisms, confinement and pseudogap, together cause the rather complicated, “insulating” $\rho_c(T)$ behavior in the cuprates, though their relative roles in determining the actual temperature dependence is not clarified yet.

Given the above-mentioned recent understanding of the c -axis transport, it is important to establish a comprehensive picture for the roles of the two mechanisms (confinement and pseudogap) in determining the temperature dependence of ρ_c and the anisotropy. For such a purpose, it is useful to elucidate the evolution of the behavior of $\rho_c(T)$, as well as the anisotropy ratio ρ_c/ρ_{ab} , over a wide range of hole doping, because T^* is known to decrease with increasing doping. In the past, there were many studies of the anisotropic resistivities in $\text{La}_{2-x}\text{Sr}_x\text{CuO}_4$ (LSCO),^{5,20,21,22} $\text{YBa}_2\text{Cu}_3\text{O}_{7-\delta}$ (YBCO),^{6,23} Bi-2212,²⁴ and BSLCO,^{4,25} but none of them cover a wide enough doping range from underdoped insulators to overdoped superconductors to yield a coherent picture.

Very recently, Komiya *et al.* measured²⁶ the anisotropic resistivity of high-quality LSCO single crystals for $x = 0.01 - 0.10$ and found that in this system the effect of pseudogap is *not* apparent (i.e., the additional mechanism to cause the insulating $\rho_c(T)$ is absent), probably because of the unique Fermi surface topology^{27,28} of LSCO. Therefore, it is useful to study another cuprate system in which one can change the hole doping over a really wide range. Obviously, BSLCO is an ideal candidate, because we have demonstrated^{29,30,31} that the hole doping can be varied (by changing the La concentration) from heavily-underdoped insulator to overdoped superconductor; moreover, ARPES measurements have found^{32,33,34} that the Fermi surface topology and the pseudogap structure of BSLCO are very similar to those of Bi-2212. We can thus expect that it is possible to sort out the respective effect of charge confinement and the pseudogap on the c -axis transport by tracing its evolution with the hole doping in BSLCO.

The purpose of this paper is to provide high-quality data, obtained from well-controlled experiments, on the evolution of the temperature dependences of ρ_c and ρ_c/ρ_{ab} of BSLCO over a wide range of doping, which give a comprehensive perspective of the origin of the unusual c -axis transport in the cuprates. Our data demonstrate that there are three different mechanisms that govern the behavior of the anisotropy ratio ρ_c/ρ_{ab} : charge confinement, pseudogap, and localization. The systematic data on the c -axis transport reported here for BSLCO and those reported by Komiya *et al.* for LSCO (Ref. 26)

will together give new bases for understanding the fundamental mechanism of the charge confinement, which is expected to be closely related to the mechanism of the high- T_c superconductivity itself.

This paper is organized as follows: Details of our crystal-growth technique to produce the high-quality BSLCO single crystals, as well as the details of our measurement technique, are presented in Section II. Section III presents our data for $\rho_{ab}(T)$, $\rho_c(T)$, and ρ_c/ρ_{ab} , putting emphasis on how they evolve with changing hole doping. The implication of the systematics of our observation is discussed in Section IV, and Section V summarizes our findings.

II. EXPERIMENTS

A. $\text{Bi}_{2-x}\text{La}_x\text{CuO}_{6+\delta}$ Crystals

The $\text{Bi}_{2-x}\text{La}_x\text{CuO}_{6+\delta}$ system is a Bi-based single-layer cuprate where the hole doping is controlled by replacing Sr with La. Until a few years ago, this material had been considered to be a particularly “dirty” system among the cuprates, because the in-plane resistivity of even the best crystal at those times showed the residual resistivities of around $70 \mu\Omega\text{cm}$ (Refs. 4,7) and the Hall coefficient R_H displayed only a weak temperature dependence,³⁵ both of which are characteristic of dirty cuprate samples.

In 1999, Ando and Murayama demonstrated²⁹ that it is possible to grow high-quality single crystals of BSLCO that show much smaller residual resistivity and a strongly temperature-dependent R_H , which conform to the “standard” behavior of cuprates. Also, though the BSLCO system was believed to possess the lowest optimum T_c among the well-studied cuprate systems, we have demonstrated³⁰ that the optimum T_c of this system can be raised to 38 K, which is almost equal to the optimum T_c of LSCO.

In BSLCO, larger La concentration x corresponds to smaller hole doping per Cu, p , and the relation between x and p , as well as the phase diagram of T_c vs p , has been sorted out³¹; it was found that optimum doping occurs at $p \simeq 0.16$ (which is achieved with $x \simeq 0.4$), but the superconductivity disappears at $p \simeq 0.10$ ($x \simeq 0.8$) upon underdoping. Low-temperature normal-state resistivity measurement of this system using 60-T pulsed magnetic field found³⁰ that the metal-to-insulator crossover occurs at $p \simeq 1/8$, below which $\rho_{ab}(T)$ shows a peculiar $\log(1/T)$ divergence.

Single crystals of $\text{Bi}_{2-x}\text{La}_x\text{CuO}_{6+\delta}$ are grown by the floating-zone (FZ) technique over a wide range of La concentration ($0.23 \leq x \leq 1.02$). Before the FZ operation, we first prepare polycrystalline rods of BSLCO. Raw powders of Bi_2O_3 , SrCO_3 , La_2O_3 , and CuO , with purities of 99.9% or higher, are dried, weighted, mixed into the nominal molar ratio of the target composition, and well ground in an agate mortar; they are then calcined at

TABLE I: Actual composition of the obtained crystals for each nominal (starting) La concentration. The molar ratios of the cations are determined by ICP-AES and are shown with the Cu value fixed to 1.

nominal La composition	Bi	Sr	La	Cu
0.20	2.02	1.70	0.23	1
0.40	1.98	1.59	0.39	1
0.50	1.99	1.52	0.49	1
0.60	1.93	1.31	0.66	1
0.70	2.00	1.30	0.73	1
0.80	2.00	1.17	0.84	1
0.90	1.92	1.06	0.92	1
1.00	1.90	0.98	1.02	1

750 – 850°C for 20 hours to form the BSLCO phase. The resulting powders are reground and calcined again, and this process is repeated twice. The x-ray diffraction analysis reveals that the powders become 100%-pure BSLCO phase after the third calcination. The resulting BSLCO powders are isostatically pressed into a rod shape ($\approx 5 \text{ mm}\phi \times 100 \text{ mm}$) and finally sintered at 850°C for 20 hours, to form a rigid polycrystalline feed rod to be used for the FZ operation.

Single-crystal growth is carried out using an infrared image furnace (NEC Machinery SC K-15HD) with two halogen lamps and double ellipsoidal mirrors. We grow BSLCO crystals with a “pure” FZ technique, which means that we do not use any solvent to reduce the temperature of the molten zone. One important technique we use is what we call “fast scan”, with which we quickly melt and quench the whole feed rod using the FZ furnace with the feed speed of 30 mm/h. This process is necessary for making the feed rod dense, which is important for avoiding the emergence of bubbles during the crystal growth; actually, the rod becomes appreciably thinner than the as-sintered rod after the fast scan (it becomes roughly $3 \text{ mm}\phi$). The “scanned” rod is then remounted to the FZ furnace and is used for the actual crystal growth. The growth rate is kept constant at 0.5 mm/h, which is two times slower than the growth rate for LSCO.²⁶ Another important technique we use during the growth is what we call “necking”; since many independent domains start to crystallize at the initial stage of the growth, after roughly 1 cm of the rod is grown, the diameter of the molten zone is gradually reduced to approximately $2 \text{ mm}\phi$, which causes fewer domains to remain in the crystal. The molten zone is then gradually fattened, which leads to the growth of the fewer domains in the resulting rod. After a few times of the necking, when the growth is successful, there remains only one domain and the whole chunk becomes a large single-domain crystal. The space around the molten zone is filled with 1 atm of flowing oxygen during the growth of underdoped crystals, while for the growth of overdoped crystals the space is filled with 1 atm of flowing air. The size of the single-domain crystals that can be obtained from the grown rod is typically $20 \times 3 \text{ mm}^2$.

TABLE II: Actual hole concentrations per Cu, p , and T_c for each La concentration x . The p values are determined from the empirical relation between x and p obtained in Ref. 31.

x	0.23	0.39	0.49	0.66	0.73	0.84	0.92	1.02
p	0.18	0.16	0.14	0.12	0.11	0.10	0.07	0.03
T_c	29	38	31	23	14	1.4	0	0

The actual La concentrations in the crystals are determined by the inductively-coupled plasma atomic-emission spectroscopy (ICP-AES). The crystals tend to contain more La than the nominal composition, but the difference is small; here we report crystals with actual x values of 0.23, 0.39, 0.49, 0.66, 0.73, 0.84, 0.92, and 1.02, and these crystals were obtained from the nominal x values of 0.20, 0.40, 0.50, 0.60, 0.70, 0.80, 0.90, and 1.00, respectively. In all these crystals, the ICP-AES analysis confirms that there is essentially no excess Bi in the crystals; rather, Bi tends to be deficient in highly La-doped crystals, as shown in Table I. On the other hand, the ratio of (Sr+La):Cu is always near 2:1.

Uniformity of the distribution of the La dopants in the crystals is confirmed by the electron-probe microanalysis (EPMA), with which the variation of the x value is estimated to be within 5%. The superconducting transition temperature T_c is determined both by the zero resistivity in the transport measurement and by the onset of the Meissner signal in the SQUID magnetization measurement; for all the crystals reported here, these two definitions give T_c values that match within $\pm 0.5 \text{ K}$, and the variation among different pieces of crystals with the same composition is also within $\pm 0.5 \text{ K}$. (Thus we refer to the T_c values with two significant digits in this paper.) The T_c values for each of the compositions are listed in Table II.

B. Measurements

The crystals are cut into dimensions of typically $2 \times 1 \times 0.05 \text{ mm}^3$ for the ρ_{ab} measurements and $1 \times 1 \times 0.05 \text{ mm}^3$ for the ρ_c measurements. Accurate determination of the crystal thickness is done by measuring the weight with $0.1 \mu\text{g}$ resolution and converting it into volume using the nominal density for each composition. We employ the straightforward four-terminal method to measure ρ_{ab} and ρ_c : For the ρ_{ab} measurements, the current contacts are painted to cover two opposing side faces of the platelet-shaped crystals to ensure a uniform current flow and the voltage contacts are painted on the two remaining side faces of the crystals. For the ρ_c measurements, two current contacts are painted to almost completely cover the opposing ab faces of the crystal and two voltage contacts are placed in the small window reserved in the center of the current contacts. In both cases, the contact pads are tactfully hand-drawn with gold paint, followed by a heat treatment at 400°C for 30 minutes

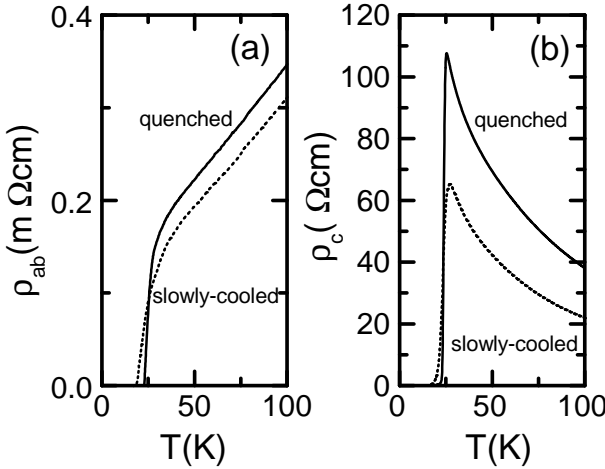


FIG. 1: Temperature dependences of (a) ρ_{ab} and (b) ρ_c of the BSLCO crystals with $x = 0.66$ ($p = 0.12$); quenched samples (solid lines) and slowly-cooled samples (dotted lines) show non-negligible difference, even though the annealing conditions are the same.

in the air, which makes the gold particles to well adhere to the sample surface. After this heat-treatment to cure the gold contact pads, the samples are annealed at higher temperatures for longer time to control the oxygen concentration; samples with x larger than 0.3 are annealed in flowing air at 650°C for 48 hours, while those with $x \leq 0.3$ are annealed in flowing oxygen at 400°C for 60 hours. In both cases, the crystals are annealed together with a sufficient amount of BSLCO powders of the same composition, and they are quenched to room temperature at the end of the annealing. Finally, gold lead wires are attached to the contact pads using silver epoxy, which is cured at relatively low temperature, 130°C . The contact resistance we achieve with this technique is less than 1Ω . We note that the above annealing conditions are chosen to minimize the superconducting transition width ΔT_c of our crystals; in all the superconducting samples, ΔT_c in $\rho_c(T)$ data is around 2 K after the above annealing.

Before finishing the description of our sample preparation technique, we would like to emphasize the importance of the quenching at the end of the high-temperature annealing. Figure 1 shows the data of $\rho_{ab}(T)$ and $\rho_c(T)$ of our BSLCO crystals with $x = 0.66$, for both quenched and slowly-cooled samples. Although both sets of the samples are annealed at 650°C for 48 hours, the data show non-negligible differences; the difference in the $\rho_{ab}(T)$ are comparatively small (the magnitude of ρ_{ab} of quenched sample is 10% larger than that of slowly-cooled sample), but the difference in $\rho_c(T)$ is significant, differing by about 50%. Also, ΔT_c is about 2 K for the quenched samples, while it is about 6 K for the slowly-cooled sample. Those differences are consistent with the interpretation that the slow cooling causes the oxygen concentration in the samples to be inhomogeneous and there are more oxygen near the surface of

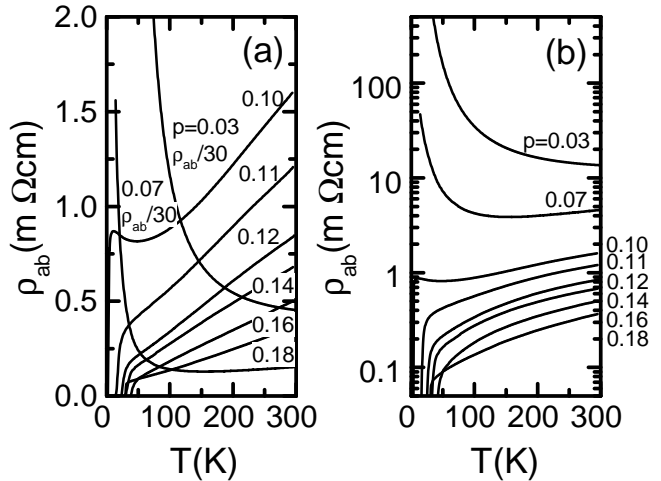


FIG. 2: (a) Temperature dependences of ρ_{ab} of the BSLCO crystals for various p . (b) Semi-logarithmic plot of $\rho_{ab}(T)$.

the slowly-cooled samples; remember that the equilibrium oxygen concentration of Bi-2201 during the annealing is dependent on both the temperature and the oxygen partial pressure, and the equilibrium concentration becomes higher as the temperature is lowered. Thus, to obtain uniformly oxygenated samples and reproducible data, quenching is indispensable.

In this work, we measure ρ_{ab} and ρ_c on more than 20 samples for each La concentration to check for the reproducibility; the variation in the absolute magnitude of the resistivity of the quenched sample is less than $\pm 10\%$, which is consistent with the size of the errors due to uncertainties in the geometrical factors.

We have previously determined the actual hole concentration per Cu, p , for various La concentrations x , and have obtained an empirical relation.³¹ In this paper we use this empirical relation to convert x into p , which are listed in Table I. Hereafter we mostly use the p value in referring to the samples, because p is much more intuitively understandable than x .

III. RESULTS

A. In-plane resistivity

Figure 2 shows the temperature dependences of ρ_{ab} for all the p values studied here. As expected (and has been reported in Refs. 29,30,31), the magnitude of $\rho_{ab}(T)$ shows a systematic increase with decreasing carrier concentration from $p = 0.18$ to 0.03. The $\rho_{ab}(T)$ curve of the overdoped sample ($p = 0.18$) shows a behavior that can be described²⁹ by $a + bT^n$ with $n > 1$, while a strictly T -linear behavior is apparent in the optimally-doped sample ($p = 0.16$). In the most underdoped non-superconducting sample ($p = 0.03$), $\rho_{ab}(T)$ shows an insulating behavior ($d\rho_{ab}/dT < 0$) from room tempera-

ture, which is quite different from the $\rho_{ab}(T)$ behavior of lightly hole-doped LSCO that shows a metallic behavior ($d\rho_{ab}/dT > 0$) even at $x = 0.01$.³⁶ We assert this difference is not intrinsic but is rather due to disorder, because the sheet resistance per CuO₂ plane of our BSLCO at $p = 0.03$ is 110 k Ω , while that of LSCO at $x = 0.03$ (Ref. 36) is only 60 k Ω ; this indicates that a significant disorder is present in the heavily-underdoped BSLCO samples. On the other hand, the residual resistivity at optimum-doping ($p = 0.16$) is only 20 $\mu\Omega\text{cm}$, indicating that the electron transport can be quite clean in this system; since we find that the crystals are morphologically very clean for both $p = 0.03$ and 0.16, the source of the electronic disorder is apparently not any crystalline defects but is likely to be the local disordering potentials due to the La dopants.

It is useful to note that the barely superconducting sample, $p = 0.10$, shows ρ_{ab} value of ~ 0.7 m Ωcm just above T_c ; this value corresponds to the sheet resistance per CuO₂ plane of 5.8 k Ω , which is almost equal to the quantum sheet resistance $h/4e^2$ ($= 6.45$ k Ω). This suggests that the disappearance of the superconductivity in BSLCO at unusually high doping of $p \simeq 0.10$ is caused by the disorder-driven superconductor-insulator transition in two-dimensional (2D) superconductors.³⁷

B. Out-of-plane resistivity

Figure 3 shows the temperature dependences of ρ_c for the same compositions as those in Fig. 2. As is the case with $\rho_{ab}(T)$, the magnitude of $\rho_c(T)$ shows a systematic increase with decreasing carrier concentration. Since the magnitude of ρ_c changes by 2 orders of magnitude from $p = 0.18$ to 0.03, the data for the overdoped and optimally-doped samples are shown in Fig. 3(a), while those of the underdoped samples are shown in Fig. 3(b), both in linear scale; Fig. 3(c) plots $\rho_c(T)$ in semi-logarithmic scale to equally show the behavior of all the samples. In Fig. 3(a), $\rho_c(T)$ data for La-free Bi_{2.13}Sr_{1.89}CuO_{6+ δ} (“pure” sample) are also shown for comparison (dotted line). It is worthwhile to note that, for each composition, the ρ_c value of our crystals is generally smaller than that reported for BSLCO in the past.^{4,25}

We note that a “metallic” temperature dependence of ρ_c is often observed, as is the case with the present experiment, in overdoped samples at high enough temperatures,^{5,6,38,39} which probably indicates that the in-plane scattering of the electrons is involved in determining the temperature dependence of ρ_c .⁴⁰ In fact, recent *c*-axis magnetoresistance study by Hussey *et al.* showed that ρ_c of LSCO is strongly affected by the scattering within the planes.⁴¹ This suggests that one may better look at ρ_c/ρ_{ab} rather than ρ_c itself to investigate the intrinsic mechanisms of the unusual *c*-axis transport, because the in-plane scattering rate is roughly cancelled out in ρ_c/ρ_{ab} .

C. Anisotropy ratio ρ_c/ρ_{ab}

Figure 4 shows the temperature dependences of the anisotropy ratio ρ_c/ρ_{ab} for all the concentrations studied. At moderate temperatures, the magnitude of ρ_c/ρ_{ab} monotonically increases with decreasing p , except for the most underdoped concentration ($p = 0.03$) at which ρ_c/ρ_{ab} suddenly drops; it is probably the case that this drop is caused by the heightened ρ_{ab} value of the $p = 0.03$ sample due to localization, and therefore if there were no enhanced disorder at this composition we would expect ρ_c/ρ_{ab} to be not much different from that for $p = 0.07$. Note that the ρ_c/ρ_{ab} value generally increases with lowering temperature, and almost reaches 10^6 just above T_c for $p = 0.10 - 0.14$.

Before our FZ-grown crystals became available, the anisotropic resistivity of BSLCO was measured by Wang *et al.* using flux-grown crystals that showed rather large residual resistivities.²⁵ Though the data by Wang *et al.* demonstrated reasonably systematic behavior and are mostly consistent with our data reported here, their data are different from ours in one important aspect: they observed that the anisotropy ratio ρ_c/ρ_{ab} is almost independent of doping at 300 K, while we observed that ρ_c/ρ_{ab} at 300 K increases systematically with decreasing p , as can be seen in Fig. 4.

We note that in the anisotropic resistivity measurements using the flux-grown crystals, it was already recognized that the BSLCO system shows a very large anisotropy ratio ρ_c/ρ_{ab} of more than 10^5 , which is the largest among the cuprates; for example, Martin *et al.* reported⁴ that ρ_c/ρ_{ab} can be as large as 3×10^5 in Bi-2201, and the work by Wang *et al.* mentioned above reported²⁵ maximum ρ_c/ρ_{ab} of 2.5×10^5 . In our crystals, perhaps because of the smaller ρ_{ab} values, the observed ρ_c/ρ_{ab} is even larger; the ρ_c/ρ_{ab} value exceeds 5×10^5 in four of the concentrations ($p = 0.10, 0.11, 0.12$, and 0.14), and the maximum ρ_c/ρ_{ab} we observe is 8×10^5 .

IV. DISCUSSIONS

In Fig. 3, one can infer that the onset of steeply insulating behavior in $\rho_c(T)$ moves to higher temperature with decreasing p in the La-doped series of samples, which is consistent with the expected behavior of the pseudogap-opening temperature T^* ; therefore, the $\rho_c(T)$ behavior clearly reflects the opening of the pseudogap. However, there is one issue that we need to elaborate on: When we estimate the actual hole concentration of the pure sample using the method we reported in Ref. 31, the p value of this pure sample is 0.17 [Fig. 5(a)]; the slope of $\rho_{ab}(T)$ also indicate that the p value of the pure samples should be around 0.17 [Fig. 5(b)]. On the other hand, compared to the La-doped $p = 0.18$ sample, the ρ_c value of the pure sample is *smaller* and the onset temperature of the insulating behavior is *lower*, both of which would normally be expected for more *overdoped*

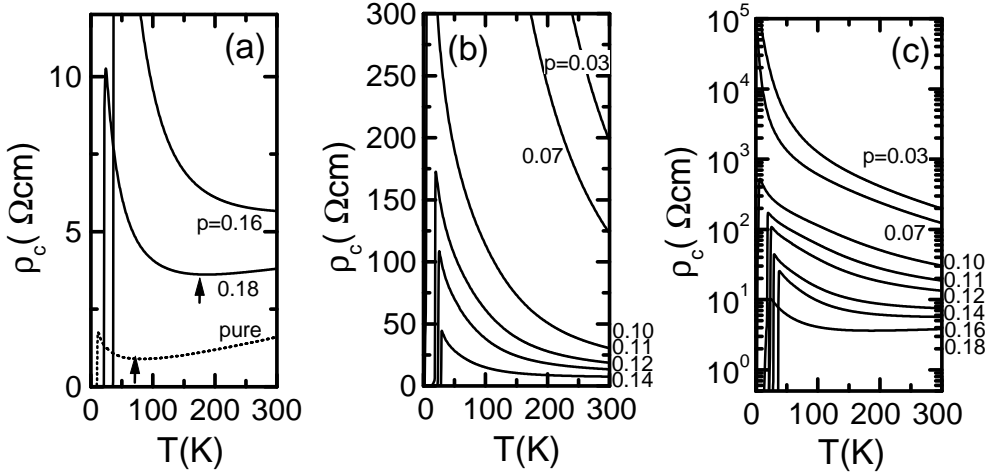


FIG. 3: Temperature dependences of ρ_c of the BSLCO crystals for (a) $0.16 \leq p \leq 0.18$ and (b) $0.03 \leq p \leq 0.14$. Panel (a) also includes $\rho_c(T)$ data of “pure” sample ($\text{La-free } \text{Bi}_{2.13}\text{Sr}_{1.89}\text{CuO}_{6+\delta}$). Arrows mark the temperature where $\rho_c(T)$ shows a minimum. (c) Semi-logarithmic plot of $\rho_c(T)$ for all the p values.

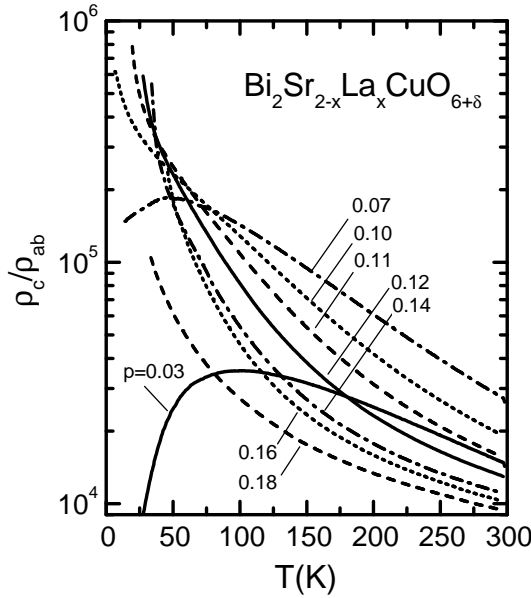


FIG. 4: Temperature dependences of ρ_c/ρ_{ab} of the BSLCO crystals calculated from the data in Figs. 2 and 3.

sample. Although this apparent puzzle looks problematic, it can be understood to be a result of a combination of extrinsic effects: First, since the constituent atoms of the apical-oxygen layer are different [$(\text{Sr},\text{La})_2\text{O}_2$ for BSLCO and $(\text{Sr},\text{Bi})_2\text{O}_2$ for pure samples], it is expected that the c -axis tunneling matrix element t_\perp is also different; it appears that t_\perp is larger in the pure samples, though the microscopic reason for the difference is not very clear. Second, since the c -axis magnetoresistance study has revealed³⁹ that in the overdoped region the pseudogap is largely due to superconducting fluctuations and thus T^* is governed primarily by T_c , the low T_c value of the pure sample is the reason for the low onset tem-

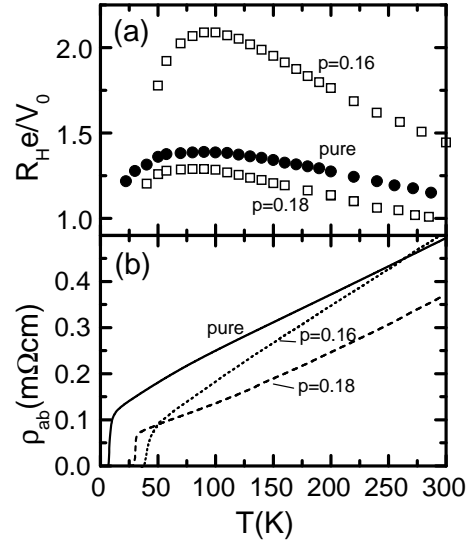


FIG. 5: (a) Plots of the renormalized Hall coefficient, $R_H e/V_0$, vs T for the pure sample and the BSCLO samples with $p = 0.16$ and 0.18 , where V_0 is the volume per one Cu atom in the unit cell; the values of $R_H e/V_0$ of various cuprates near room temperature have been found to agree for the same p value, giving a good tool to estimate p .³¹ (b) Comparison of the $\rho_{ab}(T)$ data of the pure sample to those of BSLCO with $p = 0.16$ and 0.18 .

perature of the insulating behavior.⁴²

It is useful to note that a scanning tunneling spectroscopy (STS) measurement has been done on our pure samples and the pseudogap was found to open below 68 ± 2 K.⁴³ In Fig. 3(a), the minimum in $\rho_c(T)$ of the pure sample is observed at 70 K, which perfectly agrees with T^* determined by STS and gives strong support to the interpretation that the steeply insulating behavior in $\rho_c(T)$ is largely due to the pseudogap in BSLCO as well.

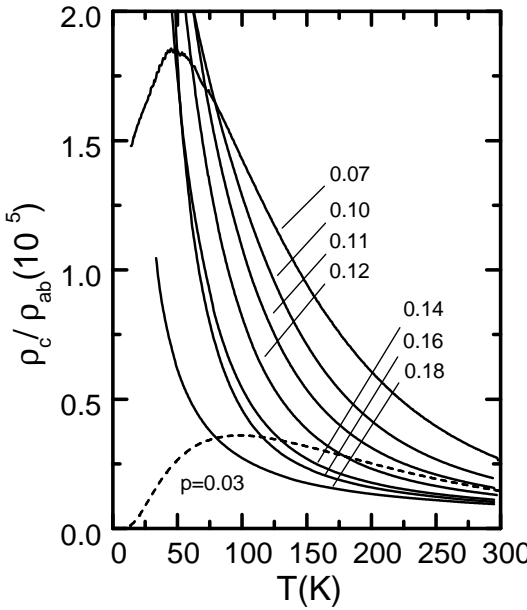


FIG. 6: Temperature dependences of ρ_c/ρ_{ab} of the BSLCO crystals plotted in linear scale.

Moreover, the STS study has concluded⁴³ that the pseudogap and the superconductivity has a common origin in the pure sample, which is in agreement with the conclusion drawn from the magnetoresistance study³⁹ for the overdoped region.

Figure 6 replots the ρ_c/ρ_{ab} data of Fig. 4 using a linear scale, which makes it easier to infer the quantitative change of the anisotropy with doping. In Fig. 6, one can see that at high temperatures the ρ_c/ρ_{ab} value drops rapidly with increasing p for $p \geq 0.07$, but this rapid change tends to saturate in highly doped samples ($p \geq 0.14$); this situation can be understood more graphically by plotting the p dependence of ρ_c/ρ_{ab} at 200 K and 300 K, as is shown in Fig. 7. It can be seen in Fig. 7 that the p dependence of ρ_c/ρ_{ab} for high doping ($p > 0.13$) is weak, while the ρ_c/ρ_{ab} values steeply increases with decreasing p for lower doping ($p < 0.13$), both at 200 K and at 300 K. It is most likely that the weak p dependence at high doping reflects the change in the strength of the charge confinement, while the steep increase in the underdoped samples reflects the enhancement of the anisotropy due to the pseudogap. Therefore, the pronounced hole-doping dependence of the anisotropy shown in Fig. 4 (or in Fig. 6) is understood to be a combined result of the confinement and the pseudogap, although quantitative separation of the two effects is difficult.

In Fig. 6, one notices that for non-superconducting concentrations ($p = 0.03$ and 0.07) there is a peak in the temperature dependence of ρ_c/ρ_{ab} (at 50 and 100 K, respectively), and below the peak temperature the anisotropy is diminished. In particular, ρ_c/ρ_{ab} for $p = 0.03$ decreases dramatically with decreasing T , suggesting that the system is heading towards an anisotropic three-dimensional (3D) state for $T \rightarrow 0$. Such dimin-

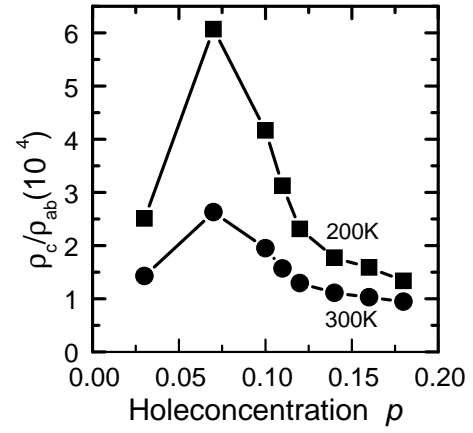


FIG. 7: p dependences of ρ_c/ρ_{ab} at 200 K and 300 K.

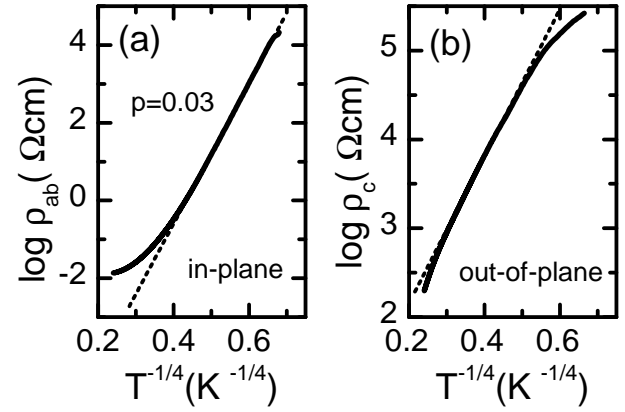


FIG. 8: (a,b) Log of $\rho_{ab}(T)$ and $\rho_c(T)$ of the BSLCO crystals at $p = 0.03$ plotted vs $T^{-1/4}$. The dotted lines are fits of the data to the variable-range hopping dependence $\rho \sim \exp[(T_0/T)^{1/4}]$.

ishment of ρ_c/ρ_{ab} has also been observed in insulating samples of Bi-2212 (Ref. 44) and LSCO (Ref. 26), and has been discussed to be due to localization of the carriers. In fact, when the carriers are completely localized and becomes immobile in *any* direction, it is natural to see the system as a “3D” insulator; note that the system is expected to retain some amount of anisotropy in the 3D-insulating state, reflecting the anisotropy of the “bare” matrix elements.

Using the resistivity data for $p = 0.03$, where the superconductivity is lost and carriers are localized due to disorder, we can actually confirm that the system is approaching a 3D insulator. Figure 8 shows the 3D variable range hopping (VRH) plots of $\rho_{ab}(T)$ and $\rho_c(T)$ for $p = 0.03$. The dotted lines are fits to the expected temperature dependence for the 3D VRH, $\rho \sim \exp[(T_0/T)^{1/4}]$. Since the 3D-VRH formula describes the temperature dependences of both ρ_{ab} and ρ_c reasonably well, one can conclude that the charge transport along *all* directions is governed by the *same* mechanism, giving a rationale to call the system to be an anisotropic 3D insulator. The fits

give T_0 values of 2.6×10^6 K and 1.4×10^5 K for $\rho_{ab}(T)$ and $\rho_c(T)$, respectively. These values are in the same range as the T_0 values obtained for flux-grown LSCO crystals in the lightly-doped regime,⁴⁵ but the source of its anisotropy is not clear at this stage.

V. SUMMARY

Systematic measurements of the resistivity anisotropy ratio ρ_c/ρ_{ab} of BSLCO over a wide doping range have documented that the anisotropy is determined by three mechanisms: charge confinement, pseudogap, and localization. At high temperature and in highly doped samples, the charge confinement is the sole determining factor, and thus we can measure the intrinsic strength of the charge confinement in this corner of the phase diagram;

our data indicate that without the effect of the pseudogap the ρ_c/ρ_{ab} value is order of 10^4 for BSLCO. At low temperature and in low doped samples, the localization governs the charge transport and the ρ_c/ρ_{ab} ratio is diminished. In underdoped superconducting samples, the pseudogap significantly enhances the ρ_c/ρ_{ab} value with decreasing temperature, causing ρ_c/ρ_{ab} to reach $\sim 10^6$. Since the effect of the pseudogap is apparently lacking in the anisotropic behavior of LSCO,²⁶ the BSLCO system offers a complementary testing ground to study the source of the peculiar c -axis transport in the cuprate superconductors.

Acknowledgments

We thank A. N. Lavrov for helpful discussions.

* ando@criepi.denken.or.jp

- ¹ For a review, see S. L. Cooper and K. E. Gray, in *Physical Properties of High Temperature Superconductors IV*, edited by D. M. Ginsberg (World Scientific, Singapore, 1994).
- ² P. W. Anderson, *Science* **256**, 1526 (1992).
- ³ W. E. Pickett, *Rev. Mod. Phys.* **61**, 433 (1989).
- ⁴ S. Martin, A. T. Fiory, R. M. Fleming, L. F. Schneemeyer, and J. V. Waszczak, **60**, 2194 (1988).
- ⁵ Y. Nakamura and S. Uchida, *Phys. Rev. B* **47**, 8369 (1993).
- ⁶ K. Takenaka, K. Mizuhashi, H. Takagi, and S. Uchida, *Phys. Rev. B* **50**, 6534 (1994).
- ⁷ Y. Ando, G. S. Boebinger, A. Passner, N. L. Wang, C. Geibel, and F. Steglich, *Phys. Rev. Lett.* **77**, 2065 (1996).
- ⁸ P. W. Anderson and Z. Zou, *Phys. Rev. Lett.* **60**, 132 (1988).
- ⁹ N. Nagaosa, *Phys. Rev. B* **52**, 10561 (1995).
- ¹⁰ E. W. Carlson, D. Orgad, S. A. Kivelson, and V. J. Emery, *Phys. Rev. B* **62**, 3422 (2000).
- ¹¹ J. Zaanen, *Science* **286**, 251 (1999).
- ¹² L. B. Ioffe and A. J. Millis, *Phys. Rev. B* **58**, 11631 (1998).
- ¹³ R. Kleiner and P. Müller, *Phys. Rev. B* **49**, 1327 (1994).
- ¹⁴ M. Tachiki, T. Koyama, and S. Takahashi, *Phys. Rev. B* **50**, 7065 (1994).
- ¹⁵ T. Timusk and B. Statt, *Rep. Prog. Phys.* **62**, 61 (1999).
- ¹⁶ M. R. Norman, H. Ding, M. Randeria, J. C. Campuzano, T. Yokoya, T. Takeuchi, T. Takahashi, T. Mochiku, K. Kadowaki, P. Guptasarma, and D. G. Hinks, *Nature (London)* **392**, 157 (1998).
- ¹⁷ T. Xiang and J. M. Wheatley, *Phys. Rev. Lett.* **77**, 4632 (1996).
- ¹⁸ M. Suzuki and T. Watanabe, *Phys. Rev. Lett.* **85**, 4787 (1999).
- ¹⁹ V. M. Krasnov, A. Yurgens, D. Winkler, P. Delsing, and T. Claeson, *Phys. Rev. Lett.* **84**, 5860 (2000).
- ²⁰ T. Kimura, K. Kishio, T. Kobayashi, Y. Nakayama, N. Motohira, K. Kitazawa, and K. Yamafuji, *Physica C* **192**, 247 (1992).
- ²¹ Y. Ando, G. S. Boebinger, A. Passner, T. Kimura, and K. Kishio, *Phys. Rev. Lett.* **75**, 4662 (1995).
- ²² G. S. Boebinger, Y. Ando, A. Passner, T. Kimura, M. Okuya, J. Shimoyama, K. Kishio, K. Tamasaku, N. Ichikawa, and S. Uchida, *Phys. Rev. Lett.* **77**, 5417 (1996).
- ²³ I. Terasaki, Y. Sato, S. Miyamoto, S. Tajima, and S. Tanaka, *Phys. Rev. B* **52**, 16246 (1995).
- ²⁴ T. Watanabe, T. Fujii, and A. Matsuda, *Phys. Rev. Lett.* **79**, 2113 (1997).
- ²⁵ N. L. Wang, B. Buschinger, C. Geibel, and F. Steglich, *Phys. Rev. B* **54**, 7449 (1996).
- ²⁶ S. Komiya, Y. Ando, X. F. Sun, and A. N. Lavrov, to appear in *Phys. Rev. B* (cond-mat/0203107).
- ²⁷ X. J. Zhou, P. V. Bogdanov, S. A. Kellar, T. Noda, H. Eisaki, S. Uchida, Z. Hussain, and Z.-X. Shen, *Science* **286**, 268 (1999).
- ²⁸ A. Ino, C. Kim, M. Nakamura, T. Yoshida, T. Mizokawa, Z.-X. Shen, A. Fujimori, T. Kakeshita, H. Eisaki, and S. Uchida, *Phys. Rev. B* **62**, 4137 (2000).
- ²⁹ Y. Ando and T. Murayama, *Phys. Rev. B* **60**, R6991 (1999).
- ³⁰ S. Ono, Y. Ando, T. Murayama, F. F. Balakirev, J. B. Betts, and G. S. Boebinger, *Phys. Rev. Lett.* **85**, 638 (2000).
- ³¹ Y. Ando, Y. Hanaki, S. Ono, T. Murayama, K. Segawa, N. Miyamoto, and S. Komiya, *Phys. Rev. B* **61**, R14956 (2000); **63**, 069902(E) (2001).
- ³² J. M. Harris, P. J. White, Z. -X. Shen, H. Ikeda, R. Yoshizaki, H. Eisaki, S. Uchida, W. D. Si, J. W. Xiong, Z. -X. Zhao, and D. S. Dessau, *Phys. Rev. Lett.* **79**, 143 (1997).
- ³³ Y.-D. Chuang, A. D. Gromko, D. S. Dessau, Y. Aiura, Y. Yamaguchi, K. Oka, A. J. Arko, J. Joyce, H. Eisaki, S.I. Uchida, K. Nakamura, and Y. Ando, *Phys. Rev. Lett.* **83**, 3717 (1999).
- ³⁴ T. Sato, T. Kamiyama, T. Takahashi, J. Mesot, A. Kaminski, J. C. Campuzano, H. M. Fretwell, T. Takeuchi, H. Ding, I. Chong, T. Terashima, and M. Takano, *Phys. Rev. B* **64**, 054502 (2001).
- ³⁵ A. P. Mackenzie, S. D. Hughes, J. R. Cooper, A. Carrington, C. Chen, and B. M. Wanklyn, *Phys. Rev. B* **45**, 527 (1992).
- ³⁶ Y. Ando, A. N. Lavrov, Seiki Komiya, Kouji Segawa, and X. F. Sun, *Phys. Rev. Lett.* **87**, 017001 (2001).
- ³⁷ Y. Fukuzumi, K. Mizuhashi, K. Takenaka, and S. Uchida, *Phys. Rev. Lett.* **76**, 684 (1996), and references therein.

³⁸ T. Watanabe, T. Fujii, and A. Matsuda, Phys. Rev. Lett. **84**, 5848 (2000).

³⁹ A. N. Lavrov, Y. Ando, and S. Ono, Europhys. Lett. **57**, 267 (2002).

⁴⁰ N. Kumar and A. M. Jayannavar, Phys. Rev. B **45**, 5001 (1992).

⁴¹ N. E. Hussey, J. R. Cooper, Y. Kodama, and Y. Nishihara, Phys. Rev. B **58**, R611 (1998).

⁴² The BSLCO samples used in Ref. 39 were taken from the same batch as the samples used in the present study, but they were annealed with different conditions; this caused the T_c values for the same composition to be lower in the samples of Ref. 39. This difference in T_c (which affects T^* in the overdoped region) is the reason for apparently different behaviors of $\rho_c(T)$ between the two studies.

⁴³ M. Kugler, O. Fischer, Ch. Renner, S. Ono, and Y. Ando, Phys. Rev. Lett. **86**, 4911 (2001).

⁴⁴ T. Kitajima, T. Takayanagi, T. Takemura, I. Terasaki, J. Phys. Condens. Matter **11**, 3169 (1999).

⁴⁵ C. Y. Chen, E. C. Branelund, C.S. Bae, K. Yang, M. A. Kastner, A. Cassanho, and R. J. Birgeneau, Phys. Rev. B **51**, 3671 (1995).